engine. Note the linear relationship between voltage and current and the resulting peak in power output when operating at matched-load conditions. Matched-load operation occurs when the load resistance equals the TEG module internal resistance. The absolute value of the slope of the voltage vs current curve is equal to the match-load resistance (in this case, approximately 33Ω).

The Ragone plot shown in Fig. 4 shows the history of the maximum installed power density for the VHHFM-2 modules with the OS MAX 61 engine. By the end of the research program, a maximum installed power density of 0.21 W/g had been achieved. Figure 4 also compares these results to different battery types, and the current break-even point of 20 min is clearly evident. Note, however, that this power output is at matched load conditions and maximum throttle setting for the engine.

The advances in power density are the result of increased power output through better module design and reduced TEG integrated assembly weight. The reduced weight is the main factor, and switching from mechanical fasteners and large heat exchanger assemblies to lightweight assemblies using adhesive and miniature heat exchangers resulted in more than 150% weight savings.

The optimum solution was found to be the use of lightweight aluminum heat exchangers (weighing fractions of a gram) along with a thermally conductive paste adhesive to hold the heat exchanger/module assembly together. A hot-side heat exchanger inserted into the muffler was usually always present as well.

Conclusions

In this research program, new high-temperature, high-efficiency microthermoelectric generator modules are developed and integrated onto unmanned microair-vehicle (MAV) propulsion systems. A $1 \times 1 \times 0.2$ cm module that produces up to 800 mW at a module thermoelectric efficiency of 6 to 7% (compared to 4% for commercially available modules) is demonstrated. The module is successfully integrated with small internal combustion engines used by developmental MAV vehicles. The maximum installed power output and power density for one of these miniature thermoelectric-generator modules was shown to be 380 mW and 210 mW/g, respectively. At this power density, TEGs outperform modern primary lithium batteries for system endurance requirements greater than 20 min.

Although there is still room for improvement, significant first steps were achieved during this research. One of the main innovations undertaken in this program was the development and integration of a small, high-performance TEG module into a system used outside of a laboratory setting. Although many advances in thermoelectric materials have been made in the past five years, little work has been performed in the area of practical research toward advanced applications of these materials outside of micropower applications. It is hoped that this work has contributed to the advancement of thermoelectric devices by focusing on the application of this technology to small-unmanned aircraft.

Acknowledgments

The work was sponsored by the Defense Advanced Research Projects Agency, Tactical Technology Office, under DARPA contract DABT63-98-C-0021 and is published with DARPA's approval. The authors would like to recognize and thank Samuel B. Wilson, III, and James McMichael of the Defense Advanced Research Projects Agency Tactical Technology Office who provided funding and guidance for this research.

References

[1]Anderson, J. D., Jr., *Introduction to Flight*, 3rd ed., McGraw–Hill, New York, 1989.

[2]Rowe, D. M. (ed.), *CRC Handbook of Thermoelectrics*, CRC Press, Boca Raton, FL, 1995.

[3]Angrist, S. W., *Direct Energy Conversion*, 3rd ed., Allyn and Bacon, Boston, MA, 1976.

[4]Johnson, D. C., "Micro Air Vehicle Missions and Technology Assessment," Lincoln Lab., Massachusetts Inst. of Technology, Project Rept. MAV-1, Lexington, MA, Nov. 1997.

Simple Trim Drag Prediction Method Based on the Biplane Theory

Kazuhiro Kusunose*
The Boeing Company, Seattle, Washington 98124-2207

Nomenclature

AR_W, AR_{CW}, AR_{TW}	=	aspect ratios defined by b_W^2/S_W, b_C^2/S_W, and b_T^2/S_W
b_W, b_C, b_T, b	=	spans of wing, canard, tail, and $\max(b_C, b_T)$
C_D, $C_{D\,\mathrm{ind}}$, $C_{D\,\mathrm{prof}}$	=	total, induced, and profile drag coefficients
$C_{D\,\mathrm{trim}}$	=	trim drag coefficient
C_L, C_{LW}, C_{LC}, C_{LT}	=	total, wing, canard, and tail lift coefficients
$C_{M\mathrm{cg}}$, C_{MWB}	=	defined by $M_{\mathrm{cg}}/qS_W\bar{c}$ and $M_{WB}/qS_W\bar{c}$ (Fig. 3)
D, D_{ind}, D_{prof}	=	total, induced, and profile drag
D_{ii}, D_{ij}	=	self- and mutually induced drag, $i, j = 1, \ldots, n$
e_W, e_C, e_T	=	Oswald's factors for wing, canard, and tail
L	=	total lift of the system
L_{wing}, L_{canard}, L_{tail}	=	lifts of wing, canard, and tail
l_C, l_T	=	distances of canard and tail from c.g. (Fig. 3)
M_{cg}	=	net pitching moment about c.g. (Fig. 3)
M_{WB}	=	wing–body pitching moment, $-L_{\mathrm{wing}}(x_W - x_{\mathrm{cg}})$
q	=	freestream dynamic pressure, $\rho_\infty U_\infty^2/2$
S_W, $\bar{c}$	=	wing reference area and wing reference chord
X, Y	=	defined in Eqs. (20) and (21)
x_W, x_{cg}	=	locations of center of pressure (wing–body) and c.g.
σ	=	interference factor (Ref. 1)

Introduction

FOR an airplane to fly with longitudinal equilibrium, it must be trimmed; the net pitching moment acting on the c.g. of the airplane must be zero. In the present analysis, we define the trim drag as the necessary induced drag penalty, or cost to the airplane of being trimmed. Classic biplane theory[1,2] is used to estimate the induced drag of multiwing configuration systems.[3,4] One obvious problem in trimming three-wing configurations is that there exist an infinite number of three-wing loading combinations that will trim the pitching moment of the system. Meredith,[4] at The Boeing Company, developed an approximation method for optimally trimming three-wing configurations. The main purpose of this engineering Note is to extend Meredith's approximation method[4] and develop a general trim-optimization method for three-wing configurations.

Discussion

According to the Helmholtz vortex theorems, the "bound vortex" of a wing cannot end at the wing tips but must continue on infinitely

Received 27 October 2003; presented as Paper 2004-0901 at AIAA 42nd Aerospace Sciences Meeting and Exhibit, Reno, NV, 5–8 January 2004; revision received 16 January 2004; accepted for publication 17 January 2004.

*Research Engineer, Acoustics and Fluid Mechanics, P.O. Box 3707, MC 67-LF; kazuhiro.kusunose@boeing.com. Member AIAA.

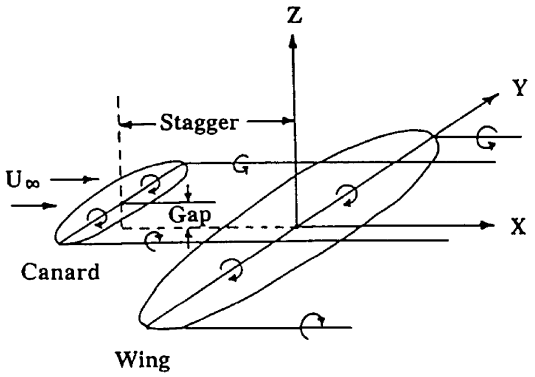

Fig. 1 Staggered biplane.

downstream as "free" vortices. It is known that these free, or trailing, vortices cause a downward velocity, generating an induced drag on the wing (self-induction). In the case of biplanes or multiplanes, the bound (or wing bound) and free vortices of one wing influence the bound vortices of the other wings, generating mutually induced drag.[1,2] Therefore, the total induced drag of a multiplane with n number of wings has $n \times n$ terms,

$$\begin{aligned} D_{\text{ind}} &= D_{11} + D_{12} + \cdots + D_{1n} \\ &\quad + D_{21} + D_{22} + \cdots + D_{2n} \\ &\quad + \cdots \\ &\quad + D_{n1} + D_{n2} + \cdots + D_{nn} \end{aligned} \tag{1}$$

D_{ii} is the self-induced drag of wing $i, i = 1, \ldots, n, D_{ij}$ is the induced drag on wing i due to the influence of wing j, $j = 1, \ldots, n$ but $j \neq i$, and D_{ji} is the drag on wing j due to the influence of wing i. In the present analysis these mutually induced drags D_{ij} and D_{ji} are estimated using the biplane theory discussed in Refs. 1 and 2. Any pair of wings is treated as a biplane, and we assume the biplane to be coplanar; that is, relative to the stagger, the gap is negligible.[3,4] (See the definitions of gap and stagger shown in Fig. 1.)

The total drag of the n-wing system can be generally expressed as the sum of the induced drag and the profile drag of the system.

$$D = D_{\text{prof}} + D_{\text{ind}} \tag{2}$$

where D_{ind} is defined in Eq. (1). The total lift of the n-wing system is the sum of the lift of each of the individual wings,

$$L = L_{\text{wing1}} + L_{\text{wing2}} + \cdots \tag{3}$$

Drag and lift coefficients are calculated by normalizing drag and lift with $q \times S_W$,

$$C_D = C_{D\,\text{prof}} + C_{D\,\text{ind}} \tag{4}$$

$$C_L = C_{L\,\text{wing1}} + C_{L\,\text{wing2}} + \cdots \tag{5}$$

To achieve longitudinal equilibrium, the n-wing system must be trimmed; the net pitching moment acting on the system must be zero. Trim drag, in general, is defined as the necessary drag penalty, or cost of the system being trimmed. It follows, then that trim drag at constant lift C_L can be calculated as the drag difference between the trimmed n-wing system and the untrimmed system. In the untrimmed system, the main wing itself is made to carry the same amount of lift C_L, either by setting the lifts of the trimming elements to be zero, or by simply using a case with just the wing and body without any trimming elements, such as canards and the tail,

$$C_{D\,\text{trim}} \equiv C_D|_{C_L} - C_D|_{C_{LW}=C_L, C_{LC}=C_{LT}=\cdots=0} \tag{6}$$

where the total lift of the trimmed n-wing system C_L is defined as

$$C_L = C_{LW} + C_{LC} + C_{LT} + \cdots \tag{7}$$

When Eq. (4) is substituted into Eq. (6) and it is assumed that the profile drags of both the trimmed and untrimmed systems are nearly equal, the trim drag at constant lift C_L reduces to

$$C_{D\,\text{trim}} = C_{D\,\text{ind}}|_{C_L} - C_{D\,\text{ind}}|_{C_{LW}=C_L, C_{LC}=C_{LT}=\cdots=0} \tag{8}$$

In other words, in this study we simply redefine the trim drag as the drag penalty due to the change in induced drag for bookkeeping purposes. Because induced drag is independent of Mach number (Ref. 5), the definition of trim drag given in Eq. (8) is valid for all transonic flows.

Two- and Three-Wing Configurations

In this section, we first consider a general three-wing configuration, such as a canard–wing–tail configuration, then treat a two-wing configuration as a special three-wing configuration case (Fig. 2).

For a three-wing configuration, total induced drag equation (1) reduces to

$$D_{\text{ind}} = D_{11} + D_{12} + D_{13} + D_{21} + D_{22} + D_{23} + D_{31} + D_{32} + D_{33} \tag{9}$$

Using the Prandtl's wing theory (see Refs. 1 and 2), we can express the self-induced drags on the main wing, canard, and tail as

$$\begin{aligned} D_{11} = L^2_{\text{wing}} \big/ \pi q b_W^2 e_W, \qquad D_{22} = L^2_{\text{canard}} \big/ \pi q b_C^2 e_C \\ D_{33} = L^2_{\text{tail}} \big/ \pi q b_T^2 e_T \end{aligned} \tag{10}$$

The values of Oswald's "wing efficiency factors" (see Ref. 6), e_W, e_C, and e_T, depend on the individual wing planforms (including wing sweep and dihedral) and the lift distributions along the wing spans, and they are generally less than one.

The mutually induced drag between the wing and canard can be expressed as

$$D_{12} = D_{21} = \sigma \frac{L_{\text{wing}} L_{\text{canard}}}{\pi q b_W b_C} \tag{11}$$

where interference factor σ depends on the sizes of span, lift distributions, and gap between the two elements.[1,2] Assuming the lift distribution of each element to be elliptical and the pair of wings

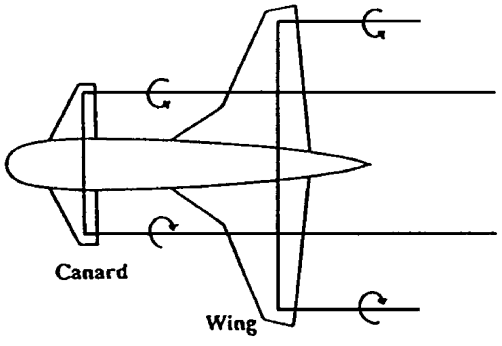

a) Canard–wing configuration

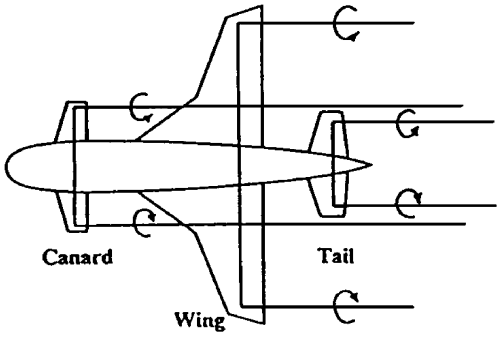

b) Canard–wing–tail configuration

Fig. 2 Two- and three-wing configuration systems.

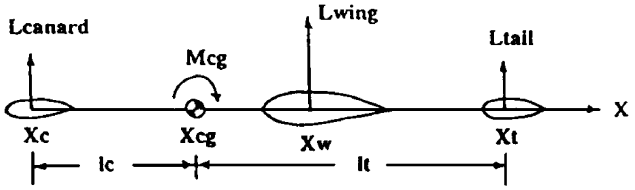

Fig. 3 Pitching moment at the c.g., canard–wing–tail configuration, $L = L_{\text{wing}} + L_{\text{canard}} + L_{\text{tail}}$; $M_{\text{cg}} = M_{wb} + L_{\text{canard}} \times l_c - L_{\text{tail}} \times l_t$ where $M_{wb} = -L_{\text{wing}} \times (X_w - X_{\text{cg}})$.

to be coplanar, for the first-order approximation, we can reduce σ: $\sigma = \min(b_W/b_C, b_C/b_W)$. (See Fig. 178 in Ref. 1). When it is further assumed that the wing span is longer than that of the canard, $b_W \geq b_C$, the total mutually induced drag becomes

$$D_{12} + D_{21} = \frac{2L_{\text{wing}}L_{\text{canard}}}{\pi q b_W^2} \tag{12}$$

Similarly, the mutually induced drag between the wing and tail and the canard and tail can be obtained as

$$D_{13} + D_{31} = \frac{2L_{\text{wing}}L_{\text{tail}}}{\pi q b_W^2}, \qquad D_{23} + D_{32} = \frac{2L_{\text{canard}}L_{\text{tail}}}{\pi q b^2} \tag{13}$$

In Eq. (13), b is defined as the larger value between b_C and b_T, and it is assumed that the spans of the canard and tail are smaller than that of the main wing ($b_C, b_T \leq b_W$).

Substituting these self-induced and mutually induced drag equations into Eq. (9), normalizing it by $q \times S_W$, and using the definition of trim drag given in Eq. (8), we obtain

$$C_{D\,\text{trim}} = \frac{C_{LW}^2 - C_L^2}{\pi \mathcal{A}\mathcal{R}_W}\frac{1}{e_W} + \frac{C_{LC}^2}{\pi \mathcal{A}\mathcal{R}_{CW}}\frac{1}{e_C} + \frac{C_{LT}^2}{\pi \mathcal{A}\mathcal{R}_{TW}}\frac{1}{e_T} + \frac{2C_{LW}}{\pi \mathcal{A}\mathcal{R}_W}(C_{LC} + C_{LT}) + \frac{2C_{LC}C_{LT}}{\pi \mathcal{A}\mathcal{R}_W}\left(\frac{b_W}{b}\right)^2 \tag{14}$$

(At constant lift condition, $C_L = C_{LW} + C_{LC} + C_{LT} = \text{const.}$)

The first step in trimming a system is examining the pitching moment acting on the c.g. of the model: The moment is defined to be positive in the pitch-up direction. As shown in Fig. 3, the normalized net moment about the c.g. is

$$C_{M\text{cg}} = C_{MWB} + C_{LC}(l_C/\bar{c}) - C_{LT}(l_T/\bar{c}) \tag{15}$$

For the system to be trimmed, the net pitching moment acting on the c.g. must be zero; setting $C_{M\text{cg}} = 0$, one obtains

$$C_{LT} = C_{MWB}/(l_T/\bar{c}) + (l_C/l_T)C_{LC} \tag{16}$$

$$C_{LW} = C_L - C_{LC} - C_{LT} = C_L - C_{MWB}/(l_T/\bar{c}) - (1 + l_C/l_T)C_{LC} \tag{17}$$

Note that the present three-wing trim drag formula will reduce to that of a two-wing configuration when we set either the canard or tail lift to be zero.

Trimming three-wing (wing–canard–tail) configurations is more complex than trimming two-wing configurations because of the infinite number of canard and tail loading combinations that can satisfy the zero pitching moment condition. For that reason, we choose a canard loading value C_{LC} that minimizes trim drag, or

$$\frac{\partial C_{D\,\text{trim}}}{\partial C_{LC}} = 0 \tag{18}$$

When the values C_L, C_{MWB}, l_C, l_T, and $\bar{c}$ are assumed to be given constants, Eq. (18) reduces to $XC_{LC} + Y = 0$. Solving this equation for C_{LC}, we obtain the optimum canard lift for minimum trim drag

$$C_{LC\,\text{opt}} = -Y/X \tag{19}$$

In Eq. (19), X and Y are defined as

$$X \equiv 1/\mathcal{A}\mathcal{R}_{CW}e_C + (1/\mathcal{A}\mathcal{R}_{TW}e_T)(l_C/l_T)^2 + (1/\mathcal{A}\mathcal{R}_W e_W) \times \left\{(1 - 2e_W)(1 + l_C/l_T)^2 + 2e_W(b_W/b)^2(l_C/l_T)\right\} \tag{20}$$

$$Y \equiv (1/\mathcal{A}\mathcal{R}_{TW}e_T)(l_C/l_T)[C_{MWB}/(l_T/\bar{c})] - (1/\mathcal{A}\mathcal{R}_W e_W) \times \Big((1 + l_C/l_T)\{C_L(1 - e_W) + (2e_W - 1)[C_{MWB}/(l_T/\bar{c})]\} - e_W(b_W/b)^2[C_{MWB}/(l_T/\bar{c})]\Big) \tag{21}$$

Given an optimum canard lift value, the tail and wing lifts can be calculated from Eqs. (16) and (17), respectively. The minimum trim drag can then be calculated using Eq. (14). Note that existence of minimum trim drag condition, $\partial^2 C_{D\,\text{trim}}/\partial C_{LC}^2 \geq 0$, can be satisfied as long as $X \geq 0$.

Because the c.g. of an airplane is not fixed (moving according to changes in airplane loading), sometimes it is more convenient to measure the locations of the canard and tail relative to a wing-fixed reference point, for example, the aerodynamic center of the wing, instead of the c.g. of the airplane. With this approach, however, we cannot obtain a simple expression for the optimum canard loading [like Eq. (19)], and the only way to obtain the optimum canard loading is by applying a numerical procedure.

Results

To validate the present trim drag prediction method for two- and three-wing configurations, predicted values were compared to experimental data from a technology concept airplane (TCA)-4 test in the NASA Langley Research Center 14 × 22 ft tunnel for high-speed-civil-transport-type configurations (given in Ref. 4). The predicted results were in good agreement with the experimental data (within 10% error range). These results, unfortunately, cannot be shown here; specific results of this TCA-4 test are considered proprietary of The Boeing Company.

Figure 4 shows a comparison of the predicted trim drag of the tested three-wing configuration with that of two different types of the tested two-wing configurations (wing–tail and wing–canard). It is clear that the use of an optimally trimmed wing–canard–tail configuration reduces trim drag (at constant lift) significantly, compared to conventional two-wing configurations.

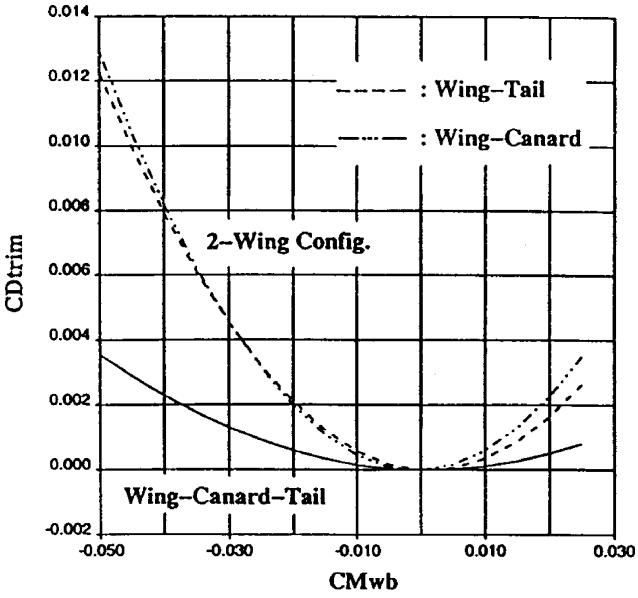

Fig. 4 Trim drag reduction using optimally trimming three-wing configuration: $C_L = 0.5$, $\mathcal{A}\mathcal{R}_w = 2.8$, $\mathcal{A}\mathcal{R}_{cw} = 0.031$, $\mathcal{A}\mathcal{R}_{tw} = 0.075$, $l_c/C_{\text{ref}} = 1.657$, $l_t/C_{\text{ref}} = 1.13$, $e_W = 0.9$, and $e_c = e_t = 0.7$.

Conclusions

General methods for predicting trim drag of two- and three-wing configurations have been developed. The classic biplane theory was used to calculate the induced drag of multiwing configuration systems. Note that the use of an optimally trimmed three-wing configuration (at constant lift) reduces trim drag significantly, compared to a conventional two-wing (wing–tail or wing–canard) configuration.

Acknowledgment

The author would like to thank P. T. Meredith of Boeing New Airplane Product Development for many valuable discussions and comments over the course of developing the present method.

References

[1]Prandtl, L., and Tietjens, O. G., *Applied Hydro- and Aeromechanics*, Dover, New York, 1957, pp. 210–219.

[2]von Mises, R., *Theory of Flight*, Dover, New York, 1959, pp. 244–250.

[3]Kendall, E. R., "The Minimum Induced Drag, Longitudinal Trim and Static Longitudinal Stability of Two-Surface and Three-Surface Airplanes," AIAA Paper 84-2164, Aug. 1984.

[4]Meredith, P. T., "Optimum Trimming of 3-Surface Configurations," Boeing Coordination Sheet, AERO-B-B156-C99-005, The Boeing Co., Seattle, WA, April, 1999.

[5]Kusunose, K., and Crowder, J. P., "Extension of Wake-Survey Analysis Method to Cover Compressible Flows," *Journal of Aircraft*, Vol. 39, No. 6, 2002, pp. 954–963.

[6]Dwinnell, J. H., *Principles of Aerodynamics*, McGraw–Hill, New York, 1949, pp. 146–149.